

Mitochondrial regular arrangement in muscle cells: a “crystal-like” pattern

Marko Vendelin ^{1,2}, Nathalie Béraud ^{1,*}, Karen Guerrero ^{1,*},
Tatiana Andrienko ^{1,3}, Andrey V. Kuznetsov ⁴, Jose Olivares ¹,
Laurence Kay ¹, and Valdur A. Saks ^{1,5}

* N.B. and K.G. participated equally in the study and are ordered alphabetically

¹ Laboratory of Fundamental and Applied Bioenergetics, INSERM E0221, Joseph Fourier University, Grenoble, France

² Institute of Cybernetics, Tallinn Technical University, Akadeemia 21, 12618 Tallinn, Estonia

³ International Biotechnological Center, Moscow State University, Moscow, Russia

⁴ Department of Transplant Surgery, University Hospital Innsbruck, Innsbruck, Austria

⁵ Laboratory of Bioenergetics, National Institute of Chemical Physics and Biophysics, Akadeemia 21, Tallinn, Estonia

Running title: Mitochondrial arrangement in muscle cells
Section: Cell physiology

ADDRESS FOR CORRESPONDENCE:

PRESENT

FROM 01.01.2005

Marko Vendelin
Laboratory of Fundamental and Applied
Bioenergetics — INSERM E0221
Université J. Fourier, BP 53
F-38041 Grenoble, France

Marko Vendelin
Institute of Cybernetics
Akadeemia 21
12618 Tallinn
Estonia

EMAIL: markov@ioc.ee

FAX: (+372) 620 4151

PHONE: (+372) 620 4169

Abstract

The aim of this work is to characterise quantitatively the arrangement of mitochondria in heart and skeletal muscles. For this, we studied confocal images of mitochondria in non-fixed cardiomyocytes and fibres from soleus and white gastrocnemius muscles of adult rats. The arrangement of intermyofibrillar mitochondria was analysed by estimating the densities of distribution of mitochondrial centres relative to each other (the probability density function). According to the found probability density functions, mitochondria are arranged in very regular manner in all studied muscles. In the cardiomyocytes (1820 mitochondrial centres marked), neighbouring mitochondria are aligned along rectangle, with distance between the centres equal to $1.97 \pm 0.43 \mu\text{m}$ and $1.43 \pm 0.43 \mu\text{m}$ in longitudinal and transversal directions, respectively. In soleus (1659 mitochondrial centres marked) and in white gastrocnemius (621 pairs of mitochondria marked), the relative distribution of mitochondrial centres is more complex. In soleus and white gastrocnemius, mitochondria are mainly organised in pairs at the level of I-band, and, due to such organisation, there are two distances characterising mitochondrial distribution in longitudinal direction in these muscles. The distance between mitochondrial centres in longitudinal direction within the same I-band is $0.91 \pm 0.11 \mu\text{m}$ and $0.61 \pm 0.07 \mu\text{m}$ in soleus and white gastrocnemius, respectively. The second distance describing mitochondrial arrangement in longitudinal direction — the distance between mitochondrial centres in different I-bands — is $\sim 3.7 \mu\text{m}$ and $\sim 3.3 \mu\text{m}$ in soleus and in gastrocnemius, respectively. In the transversal direction, the mitochondria are packed considerably closer to each other in soleus than in white gastrocnemius — the distance is equal to $0.75 \pm 0.22 \mu\text{m}$ in soleus and $1.09 \pm 0.41 \mu\text{m}$ in gastrocnemius. Our results show that mitochondria, which are situated between the myofibrils, are arranged in highly ordered crystal-like pattern in a muscle-specific manner with relatively small deviation in the distances between neighbouring mitochondria. This is consistent with the concept of the unitary nature of the organisation of the muscle energy metabolism.

Introduction

Recent studies have shown the existence of multiple specific functional interactions between mitochondria, sarcoplasmic reticulum (SR) and myofibrils in permeabilized muscle fibres (Seppet et al., 2001; Saks et al., 2001; Kaasik et al., 2001; Birkedal & Gesser, 2004). Namely, endogenous ATP has been shown to be more efficient in maintaining calcium uptake into SR than exogenous ATP (Kaasik et al., 2001). Additionally, kinetic studies have shown direct supply of endogenous ADP from ATPases to mitochondria (Seppet et al., 2001; Saks et al., 2001). Such interaction can be explained by existence of localised intracellular diffusion restrictions (Saks et al., 2003; Vendelin et al., 2004). A mild treatment of the fibres with trypsin leads to the removal of these diffusion restrictions and, at the same time, distribution of mitochondria in the fibre is changed from regular arrangement in control to random distribution after the treatment (Saks et al., 2003). Similarly, in ischemic hearts, various alterations in mitochondrial function such as the significant decrease in maximal respiration rate and half-saturation constant for ADP were observed in parallel with the changes in structural organisation of the cardiac muscle cells (Boudina et al., 2002; Kay et al., 1997b). These experimental results suggest that there is a direct link between regulation of muscle cell energetics and structural organisation of the cell (Saks et al., 2003).

According to ultrastructural electron microscopic studies, mitochondrial position in the muscle cells is rather regular and depends on the muscle type. In the heart muscle, mitochondria are arranged in longitudinal lattice between the myofibrils and are located within the limits of the sarcomeres (Sommer & Jennings, 1986; Segretain et al., 1981). The correlation between sarcomere and mitochondrial length is preserved during the heart muscle contraction or when the muscle is stretched (Nozaki et al., 2001). In white and

red skeletal muscles, mitochondria are either arranged in pairs on both sides of Z-line or form columns in longitudinal direction in interfilament space (Ogata & Yamasaki, 1985, 1997). Thus, the arrangement of mitochondria is rather repetitive and similar for each sarcomere. According to the studies using fluorescence recovery technique, mitochondria are morphologically and functionally heterogeneous in number of cells (Collins et al., 2002). In cardiac muscle mitochondria present single poorly branching organelles in normal conditions (Bakeeva et al., 1983). In hypoxic conditions, cardiac mitochondria can fuse together to form gigantic mitochondria which are longer than several sarcomeres (Sun et al., 1969). This is one of the examples showing that mitochondrial morphology is a dynamic process which is regulated by the balance of fission and fusion and this balance can be changed by such interventions as hypoxia (Collins et al., 2002; Rube & van der Bliek, 2004).

In all these studies, however, mitochondrial distribution has not been analysed quantitatively. Such quantitative description is required to relate the structural organisation of the muscle cells to interactions between mitochondria and intracellular ATP-consuming systems and, thus, to the intracellular energy crosstalk. Additionally, fixed preparations have been used in the cited ultrastructural studies and, depending on the procedures used in freezing and preparing the fibres, the fixation might influence the results (Roy et al., 1996).

The aim of this work is to analyse quantitatively the arrangement of mitochondria in heart and skeletal muscles. In this work, confocal images of non-fixed cardiomyocytes and fibres from soleus and white gastrocnemius muscles were analysed by an algorithm for this purpose. The position of mitochondria relative to each other in different muscles were described by probability density functions. The results show ordered (crystal-like)

arrangement of mitochondria with different distribution functions in various muscle cells. This approach may be used for analysis of structural and functional changes in muscle cells in different physiological and pathophysiological states.

Methods

Animals

Adult Wistar rats (male ~300 g and female ~240 g) were used in all experiments. The investigation conforms with the *Guide for the Care and Use of Laboratory Animals* published by the National Institutes of Health (NIH Publication No. 85-23, revised 1985).

Preparation of skeletal muscle fibres

The fibres were prepared from adult female Wistar rat white gastrocnemius and soleus muscles. Fibres were stored and imaged in solution A (for composition see below) in the presence of exogenous substrates (glutamate 5 mM and malate 2 mM). The preparation of the fibres has been described earlier (Saks et al., 1998).

Preparation of isolated cardiomyocytes

Intact cardiomyocytes were isolated from adult male Wistar rat heart as described by Kay et al. (1997a).

Confocal microscopy

Two independent methods were used to visualise the mitochondrial position in the non-permeabilized muscle fibres and cardiomyocytes.

Imaging of mitochondrial calcium by Rhod-2 AM. Rhod-2 AM is a cell permeable fluorescent probe for mitochondrial matrix Ca^{2+} . Non-permeabilized muscle fibres were incubated in Multidish 24 wells (from Nunc A/S, Roskilde, Denmark) with 5 μM of Rhod-2 AM in solution A for ~1 hour at 4°C in the presence of exogenous substrates (glutamate 5 mM and malate 2 mM). Rhod-2 AM has a rhodamine-like fluorophore whose excitation and emission maxima are 557 nm and 581 nm, making it convenient to use with Ar and

Kr lasers as an excitation source.

Imaging of mitochondria using MitoTracker(R) Red CMXRos. MitoTracker(R) Red CMXRos is a derivative of x-rosamine and specifically binds to mitochondria. The fluorescence of this dye was measured (excitation and emission maxima at 579 nm and 599 nm, respectively). Non-permeabilized muscle fibres were incubated in Multidish 24 wells (from Nunc A/S, Roskilde, Denmark) with 100 nM of MitoTracker(R) Red CMXRos in solution A for 2 hours at 4°C in the presence of exogenous substrates (glutamate 5 mM and malate 2 mM). Cardiomyocytes were incubated with MitoTracker(R) Red CMXRos for 45 min at 37°C in Flexiperm(R) chambers (from Vivascience, Hanau, Germany) in solution A with 5 mM glutamate and 2 mM malate.

Muscle fibres and cardiomyocytes were mounted in Flexiperm(R) slides (from Vivascience, Hanau, Germany) in the presence of solution A as follows. Muscle fibres were put on a slide, stretched slightly before fixing the ends of the muscles by attaching Flexiperm(R) micro12 to the slide. Then the solution A was added to each chamber of Flexiperm(R) micro12 which contained the fibre. In the case of cardiomyocytes, Flexiperm(R) micro12 was attached to the slide first, then solution A and cardiomyocytes were added to a chamber.

All preparations were imaged using a confocal microscope Leica DM IRE2 (from Leica microsystems, Heidelberg, Germany) with a 63X water immersion objective lens (NA 1.2). The use of such a water immersion prevented from geometrical aberrations.

Solutions

Solution A contained, in mM: CaK₂EGTA 2.77, K₂EGTA 7.23 (free calcium concentration $\sim 0.1 \mu\text{M}$), MgCl₂ 6.56, dithiothreitol (DTT) 0.5, potassium 2-(N-morpholino)ethanesulfonate (K-MES) 53.3, imidazole 20, taurine 20, Na₂ATP 5.3, phosphocreatine

15, pH 7.1 adjusted at 25°C.

All reagents were purchased from Sigma (Saint Louis, MO, USA) except ATP, which was obtained from Boehringer (Germany).

Quantitative analysis of mitochondrial positioning

To analyse how mitochondria are positioned relative to each other, the confocal images of the skeletal muscle fibres and cardiomyocytes were used with easily distinguishable mitochondria. Each image was rotated until the muscle fibre or cell was oriented in vertical direction, judged by eye. Next, the centres of mitochondria were marked manually. For each mitochondrion, the closest mitochondrial centres were found among mitochondria in several sectors as shown in Fig. 1. Then, the relative coordinates of the closest neighbours were computed.

Before the analysis, the relative coordinates of the closest neighbours have been corrected as follows.

In cardiomyocytes, the local myofibrillar orientation was estimated and accounted for. Since contractile apparatus in the cardiac muscle is widely branching, one has to take into account such organisation of the muscle before the distances between any two points in the cell are measured (Sommer & Jennings, 1986). For each mitochondrial centre, we approximated local myofibrillar orientation by fitting with the straight line the positions of mitochondrial centre and the centres of its two neighbours found in the sectors aligned along the fibre. The fitting was performed using the least-squares method. The obtained line was considered as a local orientation of myofibrils and all the neighbouring mitochondria were rotated to orient the line vertically. The relative coordinates obtained after rotation were stored and analysed statistically (see below).

In soleus and gastrocnemius, mitochondria form lines which were not exactly perpen-

dicular to fibre orientation (Fig. 2B and Fig. 2C). Since the angle between the lines formed by mitochondria and the fibre orientation was different in different fibres and even in the different sections of the same fibre, we transformed the relative mitochondrial positions as follows. First, for each mitochondrial centre, we approximated local orientation of the “mitochondrial line” by fitting with the straight line the positions of mitochondrial centre and the centres of its two neighbours found in the sectors aligned across the fibre. The fitting was performed using the least-squares method. Second, new relative coordinates of mitochondrial neighbours were computed by reducing the coordinate value along the fibre by factor $x \cdot \sin \alpha$, where x is the relative coordinate of neighbour mitochondria in transversal direction and α is an angle between the transversal direction and the found local “mitochondrial line” direction. Thus, the mitochondrial neighbours were sheared to form the “mitochondrial line” which was perpendicular to the fibre. The relative coordinates obtained after such transformation were stored and analysed statistically (see below).

The statistical analysis was performed by computing distribution function of the distance between the centres of neighbour mitochondria as well as by computing probability density functions. The both functions (distribution and probability density) were computed for each sector separately. In the analysis, the values are expressed as $\text{mean} \pm \text{SD}$.

The programs developed for this analysis were written in Python and are available on request.

Results

The representative confocal images of non-fixed intact cardiomyocytes and skeletal muscle fibres are shown in Fig. 2.

Cardiomyocytes. A representative confocal image of non-permeabilized cardiomyocyte with marked mitochondria is shown in Fig. 3. In Fig. 4, the distances between mitochondrial centres taken from image in Fig. 3 are analysed. According to our analysis (Fig. 4A), the distances between mitochondrial centres are smallest in the direction transversal to the fibre. The largest distances are in diagonal direction (angle 45°). The distribution can be presented in radial plot, where the average distance between mitochondrial centres is related to direction between mitochondria. In this plot, the distances between the centres are given by the distances from the reference point (coordinates 0, 0) plotted in the direction corresponding to each sector (Fig. 4B). From inspection of radial plot (Fig. 4B), it is clear that mitochondrial centres are not distributed randomly, but arranged according to some regular pattern. Indeed, if mitochondria would be distributed randomly, the mean distance as well as the distribution functions would not depend on direction and, in radial plot, the centres would have been aligned along a circle.

In the analysis presented in Fig. 4, only the distances between mitochondrial centres within each sector (see Fig. 1 for definition of the sector) are taken into account. To distinguish the distributions of mitochondrial centres in each of the sectors, we computed the probability density functions for mitochondrial centres in each of the sectors (Fig. 5) using confocal images ($n = 10$) of cardiomyocytes with total 1820 mitochondrial centres marked. According to computed probability density function, the mitochondrial centres are packed in certain areas within the sectors. The areas with the highest probabilities are aligned along rectangle with the longer side of rectangle aligned along the fibre (Fig.

5).

Since the distances between mitochondrial centres are not the same in the direction along and perpendicular to the fibre, considerable amount of mitochondrial centres are located near the borders of 45° sectors (Fig. 5). Taking into account that the distance between mitochondrial centres in diagonal direction is usually larger than that in longitudinal or transversal directions, the mitochondrial centres in diagonal direction are not accounted for by our algorithm if the centre is positioned in the different sector. To avoid such interaction of mitochondria in different sectors, the sectors were adjusted as follows: the sectors in longitudinal direction were taken equal to 30° , in the transversal direction equal to 60° , and 45° in the diagonal direction. The probability density functions corresponding to adjusted partitioning of the neighbouring mitochondria to the sectors is shown in Fig. 6.

The regular (crystal-like) arrangement of mitochondrial centres is clear from the mean positions of mitochondrial centres (Fig. 6B). The mean positions are aligned along rectangle, with longer distances between mitochondrial centres along the fibre. Using the same partitioning to the sectors as in Fig. 6, the following distances between mitochondrial centres were found: $1.97 \pm 0.43 \mu\text{m}$ and $1.43 \pm 0.43 \mu\text{m}$ in longitudinal and transversal directions, respectively.

Soleus. In skeletal muscle, mitochondrial arrangement is different from that of cardiomyocytes with the most of the mitochondria arranged in pairs in soleus (Fig. 2). In our analysis, we marked only mitochondria which were seen as a spots in the image (indicated by arrows in Fig. 2B) and ignored the long mitochondria which were connecting the mitochondrial pairs in longitudinal direction (marked by arrowheads in Fig. 2B). Such approach was used since it is impossible to distinguish whether the connection between

pairs of mitochondria is formed by separate but not resolved mitochondria or by long extensions of mitochondria within the pairs. An example of the confocal image of soleus fibre with marked mitochondrial centres is shown in Fig. 7. Since the arrangement of mitochondria in soleus is different from the one in cardiomyocytes, there are large differences in distribution of mitochondrial centres relative to each other in these muscles. These differences were taken into account as follows.

To determine how the neighbouring mitochondria should be partitioned to represent the spacial distribution of mitochondria in soleus, we analysed in detail the distribution of all marked mitochondria shown in Fig. 7. As a first step of our analysis, we found, for each marked centre, the neighbouring mitochondria which were positioned within $5\ \mu\text{m}$ in longitudinal and transversal directions, i.e. within $5\ \mu\text{m} \times 5\ \mu\text{m}$ box. The size of the box was selected to cover more than one sarcomere length in the muscle. Next, the probability density function describing *all neighbour mitochondria* was computed (Fig. 8A). Since this probability density function describes not only the closest mitochondrial neighbours (as in Fig. 5), but all neighbours that lie in $5\ \mu\text{m} \times 5\ \mu\text{m}$ box, there are several maxima of probability density function in each direction. Since these maxima are distributed quite symmetrically relative to the reference point (cross in Fig. 8), it is sufficient to recognise the origin of the maxima located in one quarter of the plot only. The origin of marked maxima in positive transversal and longitudinal directions is indicated in the scheme in Fig. 8B. For example, the maximum marked with “5” in Fig. 8A corresponds to the neighbouring mitochondria in transversal directions. Since the both mitochondria within the pair usually have neighbours in transversal direction, this maximum is considerably larger than the maximum marked with “6” in Fig. 8. Other maxima produced by the both mitochondria within the pair are marked with “3” and

“8”. Note that these maxima are considerably larger (presented by brighter spots in Fig. 8A) than the others (compare with maxima 2, 4, 6, 7, and 9) in the map (Fig. 8A). In longitudinal direction, the maxima (1, 2, 3, and 4) are clearly separated from each other due to the small relative variation in the distances between mitochondrial centres in this direction. In transversal direction, the maxima corresponding to the closest neighbours (5, 6, 7, 8, 9) are distinguishable but not as clearly as in the longitudinal direction. The maxima, corresponding to the neighbouring mitochondria which are further away in transversal direction from the centre, are fused together leading to the formation of lines in Fig. 8A. This indicates that the relative variation of distances in transversal direction is considerably larger than in the longitudinal one.

To describe the distribution of mitochondria in soleus, we determined the distribution mitochondrial neighbours corresponding to maxima 1, 2, 5, 6, and 7 in Fig. 8 and their symmetric reflections. Indeed, mitochondria positioned near these maxima determine the characteristic distance in transversal direction (arrow 5 in Fig. 8B) as well as the both characteristic distances in longitudinal direction (arrows 1 and 2 in Fig. 8B). The probability density function corresponding to such partitioning of neighbours into sectors is shown in Fig. 9. The probability density function was found using $n = 10$ confocal images with total 1659 mitochondrial centres marked. Note that variance of the distances is considerably larger in transversal than in longitudinal direction (Fig. 9A). The distances between centres of neighbouring mitochondria are as follows: $0.91 \pm 0.11 \mu\text{m}$, $2.83 \pm 0.65 \mu\text{m}$, and $0.75 \pm 0.22 \mu\text{m}$ corresponding to distances 1, 2, and 5 in Fig. 8B.

White gastrocnemius. In white gastrocnemius, most of the mitochondria are arranged in pairs, similar to soleus (Fig. 2). As for soleus, we marked only mitochondria which were seen as a spots in the image (indicated by arrows in Fig. 2C) and ignored the long

mitochondria which were either connecting the pairs in longitudinal direction (marked by arrowheads in Fig. 2C) or in transversal direction (marked by “*” in Fig. 2C).

Since the distances between mitochondria within each of the pairs is considerably smaller than in soleus (see below), we were not able to distinguish the mitochondria within the pairs in most of our images. For this reason, we analysed the distances between *pairs of mitochondria*, marking the centre of each pair as shown in Fig. 10. The probability density function and used partitioning of the neighbouring pairs to the sectors is shown in Fig. 11. As in the case of oxidative muscles analysed earlier, the mitochondrial pairs are positioned rather regularly in white gastrocnemius. The distances between the pairs of mitochondria are as follows: $3.33 \pm 0.96 \mu\text{m}$ and $1.09 \pm 0.41 \mu\text{m}$ in longitudinal and transversal directions, respectively. According to the Welch test, the mean distance obtained for transversal direction is considerably larger ($p < 0.001$) than the same distance in soleus ($0.75 \pm 0.22 \mu\text{m}$, distance 5 in Fig. 8B). The difference between the mean transversal distances in soleus and white gastrocnemius is $0.31\text{--}0.38 \mu\text{m}$ (95% confidence interval).

In some confocal images we were able to distinguish mitochondria within the pairs. According to our data (10 images with 85 distances found), the distance between the mitochondrial centres in pairs is $0.61 \pm 0.07 \mu\text{m}$. Note that the mean value of this distance is considerably smaller (the Welch test, $p < 0.001$) than the one found for soleus ($0.91 \pm 0.11 \mu\text{m}$, distance 1 in Fig. 8B). The difference between the mean distances between mitochondria in pair in white gastrocnemius and soleus is $0.28\text{--}0.31 \mu\text{m}$ (95% confidence interval).

Discussion

In this work, the arrangement of mitochondria within the muscle was assessed by analysing quantitatively the distances between mitochondrial centres. To our knowledge, this is the first time when the positions of neighbouring mitochondria are characterised by probability density functions in the muscle cells. Analysis of confocal images of non-fixed cardiomyocytes and skeletal muscle fibres by this method reveals that intermyofibrillar mitochondria are arranged in highly ordered pattern (crystal-like) with relatively small deviation in the distances between neighbouring mitochondria in cardiac and skeletal muscles. Moreover, this arrangement is a muscle specific.

According to ultrastructural studies of cardiac muscle, mitochondria occupy about 30-35% of myocardial cell volume (McCallister & Page, 1973; Bossen et al., 1978; Sommer & Jennings, 1986; Schaper et al., 1985) and are distributed everywhere in the cell (Sommer & Jennings, 1986). Intermyofibrillar mitochondria usually do not violate the limits of sarcomeres and are located between the zone demarcated by two Z lines (Muir, 1967; Segretain et al., 1981; Shimada et al., 1984; Sommer & Jennings, 1986). Thus, in longitudinal direction, the distance between the centres of two neighbouring mitochondria is expected to be similar to the sarcomere length. From our analysis, this distance is $\sim 2 \mu\text{m}$ and is close to the measured sarcomere length value in relaxed state (Sommer & Jennings, 1986). In transversal direction, it has been suggested that all contractile material is within $0.5 \mu\text{m}$ of mitochondria in cardiac muscle (Sommer & Jennings, 1986). Taking the maximal diameter of myofibril equal to $1 \mu\text{m}$, we obtain that the distance between the centres of neighbouring mitochondria in transversal direction should be larger than $1 \mu\text{m}$ by a diameter of mitochondria. The mean distance found in our study ($\sim 1.5 \mu\text{m}$) suggests that the diameter of mitochondria is at least $\sim 0.5 \mu\text{m}$ in non-fixed preparations.

In the skeletal muscle, intermyofibrillar mitochondria are arranged in register with the sarcomere. In red fibres, mitochondria form either pairs on the both sides of Z-line or columns on A-band level (Ogata & Yamasaki, 1985, 1997). In white fibres, most of mitochondria are organised in pairs next to Z-line and rather few are located between Z-lines in the form of thin columns (Ogata & Yamasaki, 1985, 1997). The same pattern of mitochondrial arrangement is evident from the confocal images of the skeletal muscles using specific fluorescent markers (Figs. 2, 7). In some images, thin links between the bright spots can be identified (arrowheads in the insets of Fig. 2B and Fig. 2C), corresponding to the “column-forming” mitochondria of Ogata & Yamasaki (1985). Additionally, long pairs of mitochondria running along I-band (see mitochondria marked by “*” in Fig. 2C) were observed in white gastrocnemius, in agreement with the earlier studies (Ogata & Yamasaki, 1985, 1997). In our analysis, we did not consider the thin columns or pairs of mitochondria (marked by arrowheads and “*” in Fig. 2), but marked only the centres of mitochondria within the pairs along I-band. Such method was used since it is hard to distinguish whether these long structures are formed by separate mitochondria or long extensions of mitochondria (Fawcett & McNutt, 1969) within the marked bright spots in I-band limited mitochondria. Thus, the distances analysed in skeletal muscle represent the distances between the mitochondria forming pairs on the both sides of Z-line.

On the basis of our images, we conclude that the pattern of mitochondrial arrangement is similar in soleus (mainly oxidative muscle) and white gastrocnemius (mainly glycolytic muscle). This is in contrast with the differences in the regulation of respiration by exogenous ADP: in oxidative skeletal muscles the affinity for ADP is very low (apparent K_m very high), while in glycolytic muscle the mitochondrial affinities for ADP is very high *in vivo* and *in vitro* (Veksler et al., 1995; Kuznetsov et al., 1996). Thus, regardless to the

differences in the participation of mitochondria in energy crosstalk in these two muscle types, mitochondria are arranged in similar and highly ordered manner. In longitudinal direction, the distances between two pairs of mitochondria are similar for soleus (sum of the distances corresponding to maxima 1 and 2 in Fig. 8, $\sim 3.7 \mu\text{m}$) and white gastrocnemius (the distance between the pairs, $\sim 3.3 \mu\text{m}$) and, according to the ultrastructural studies, correspond to the distances between two Z-lines. Since we stretched the skeletal muscle fibres when mounting on a microscopic slide (see Methods), the sarcomere length is somewhat larger than the one attributed to physiological conditions (Burkholder & Lieber, 2001) and correspond to the descending limb in force-length relationship (Rassier et al., 1999). The main difference between the soleus and white gastrocnemius is in the distances between mitochondrial centres within the same I-band. Namely, in longitudinal direction, mitochondrial centres are considerably closer to each other in white gastrocnemius muscle than in soleus, leading to the reduced width of “mitochondrial band” covering each Z-line in white gastrocnemius. In transversal direction, the distances between mitochondrial centres is considerably smaller in soleus than in white gastrocnemius pointing to the higher density of mitochondria in soleus.

Most of the ultrastructural studies of the mitochondrial arrangement in the muscle cells have been performed on the fixed and frozen material. Depending on the procedures used in freezing and preparing the fibres, the results of cellular volume assessments can vary more than 50% (Roy et al., 1996). In our study, we were able to analyse the mitochondrial distribution in non-fixed fibres surrounded with solution containing substrates. The fibres or cells were isolated to investigate them using confocal microscopy, but the intracellular environment was kept, similar to the recent studies on nuclear patterning in living muscle cells in the intact animal (Bruusgaard et al., 2003). Since there is no fixation involved,

our technique allows to study quantitatively alteration in mitochondrial distribution in response to the changes of physiological state of the same fibre or cell, i.e. in fully functional mitochondria.

There is an important difference between mitochondrial distributions in cardiac muscle cells observed using electron and confocal microscopy. Usually, the images obtained by electron microscopy from the thin sections of cardiac muscle show larger amount of irregularities in position of intermyofibrillar mitochondria than the images obtained by confocal microscopy. For example, it is common that there are several mitochondria packed together between sarcomeres (Fawcett & McNutt, 1969; Forbes & Sperilakis, 1984; Sommer & Jennings, 1986). The confocal images of cardiac muscle cells show remarkable regularity in arrangement of mitochondria between myofibrils (Duchen, 1999). The regular arrangement of mitochondria in confocal images of cardiac muscle has been demonstrated by cross-correlating the fluorescence images of flavoprotein (autofluorescence) and tetramethylrhodamine ethyl ester (mitochondrial inner-membrane potential sensitive dye). (Romashko et al., 1998). Namely, such cross-correlation map has several peaks which are regularly spaced in longitudinal and transversal directions. If a central peak in the cross-correlation map represents the coincidence of the both images then peripheral peaks observed in the map indicate the periodicity of the packing of mitochondria along myofibrils (Romashko et al., 1998). Recently, Aon et al. (2004) used the regularity of mitochondrial positioning in the cardiac cell by dividing the image of the cell with the grid filled with small squares ($\sim 2 \times 2 \mu\text{m}$) and analysing the fluorescence within each of the squares. Using such approach, usually 1-2 mitochondria were observed in each square of the grid (Aon et al., 2004). The reasons for such difference between mitochondrial distribution accessed by electron microscopy and confocal microscopy are not clear. One of the possible expla-

nations is that when thin sections is analysed, as in electron microscopy, mitochondrion can be either left out from the section by very small margin or have several membrane invasions which split a mitochondrion into several in the image plane. Additionally, fixation procedures used in electron microscopy may play a role here. Alternatively, several mitochondria could be represented by a single bright spot in confocal images due to the resolution limits of confocal microscopy. Whether any of these explanations is a correct one or not, is not clear and requires further investigation.

Our study has an important limitation. Namely, we used only one section in our analysis and not the series of sections covering three-dimensional bulk of tissue. In confocal images, the fluorescent signal is detected from rather thick section, $> 0.3\mu\text{m}$ (given for emission at 488 nm) due to the limitation in resolution. Thus, the distances which we compute are projections from three-dimensional space to our image plane leading to some underestimation of these distances. To overcome this limitation, the series of images must be acquired covering the three-dimensional area of interest and analysed to reveal three-dimensional organisation of mitochondria in the cells. Such extension of our method is in development.

The regular arrangement of mitochondria in the heart muscle cells is in accordance with the recently described functional interactions between mitochondria and myofibrillar and sarcoplasmic reticulum ATPases (Seppet et al., 2001; Saks et al., 2001; Kaasik et al., 2001; Birkedal & Gesser, 2004). Already in the 1960s, the even distribution of mitochondria in the cross-sections of heart muscles led to the following suggestion: “each mitochondrion serves only a very limited area of the myofilament mass immediately surrounding it” (Fawcett & McNutt, 1969). As it was pointed out by Sommer & Jennings (1986), the close association of mitochondria with other intracellular structures must not

be taken as prime evidence for specific functional interaction since the amount of mitochondria is very large in the cardiac cells. However, there is a kinetic evidence for such interactions from the experiments on permeabilized cardiac fibres: (a) it is impossible to inhibit completely mitochondrial respiration when stimulated by endogenous ATPases using externally added ADP-trapping system as long as the intracellular structures are kept intact (Seppet et al., 2001; Saks et al., 2001); (b) Ca^{2+} uptake can be enhanced by endogenous rephosphorylation of ADP to ATP either using endogenous creatine kinase or oxidative phosphorylation as compared to exogenous ATP (Kaasik et al., 2001). The interaction between mitochondria and ATP-consuming systems can be explained by local intracellular diffusion restrictions which divide the cell into unitary structures containing mitochondrion and enzymatic systems consuming ATP next to the mitochondrion, such as sarcoplasmic reticulum and actomyosin ATPases (Saks et al., 2001, 2003; Vendelin et al., 2004). The crystal-like arrangement seen in our work is consistent with this hypothesis and suggests the unitary structure of the studied muscle cells. Implications of such unitary structure to regulation of oxidative phosphorylation within units as well as synchronisation of events in these units within the cell are not clear and are subject of active research (Vendelin et al., 2000; Saks et al., 2004; Aon et al., 2003, 2004).

In conclusion, our results show that mitochondria, which are situated between the myofibrils, are arranged in highly ordered crystal-like pattern in a muscle-specific manner with relatively small deviation in the distances between neighbouring mitochondria. This is consistent with the concept of the unitary nature of the spacial organisation of the muscle energy metabolism. The developed method may be used for relating structural and functional changes in muscle cells in several physiological and pathophysiological states.

Acknowledgements

We would like to thank Joëlle Demaison and Serge Soyez (Joseph Fourier University, Grenoble) for technical assistance; and Dr. Frédéric de Oliveira for discussions and his kind gift (MitoTracker(R) Red CMXRos). This work was supported in part by Marie Curie Fellowship of the European Community programme “Improving Human Research Potential and the Socio-economic Knowledge Base” (M.V., contract No HPMF-CT-2002-01914).

References

- Aon MA, Cortassa S, Marban E & O'Rourke B (2003). Synchronized whole cell oscillations in mitochondrial metabolism triggered by a local release of reactive oxygen species in cardiac myocytes. *J Biol Chem* **278**, 44735–44744.
- Aon MA, Cortassa S & O'Rourke B (2004). Percolation and criticality in a mitochondrial network. *Proc Natl Acad Sci U S A* **101**, 4447–4452.
- Bakeeva LE, u S Chentsov Y & Skulachev VP (1983). Intermitochondrial contacts in myocardiocytes. *J Mol Cell Cardiol* **15**, 413–420.
- Birkedal R & Gesser H (2004). Regulation of mitochondrial energy production in cardiac cells of rainbow trout (*Oncorhynchus mykiss*). *J Comp Physiol [B]* **174**, 255–262.
- Bossen EH, Sommer JR & Waugh RA (1978). Comparative stereology of the mouse and finch left ventricle. *Tissue Cell* **10**, 773–784.
- Boudina S, Laclau MN, Tariosse L, Daret D, Gouverneur G, Bonoron-Adele S, Saks VA & Santos PD (2002). Alteration of mitochondrial function in a model of chronic ischemia in vivo in rat heart. *Am J Physiol Heart Circ Physiol* **282**, H821–H831.
- Bruusgaard JC, Liestol K, Ekmark M, Kollstad K & Gundersen K (2003). Number and spatial distribution of nuclei in the muscle fibres of normal mice studied in vivo. *J Physiol* **551**, 467–478.
- Burkholder TJ & Lieber RL (2001). Sarcomere length operating range of vertebrate muscles during movement. *J Exp Biol* **204**, 1529–1536.
- Collins TJ, Berridge MJ, Lipp P & Bootman MD (2002). Mitochondria are morphologically and functionally heterogeneous within cells. *EMBO J* **21**, 1616–1627.
- Duchen MR (1999). Contributions of mitochondria to animal physiology: from homeostatic sensor to calcium signalling and cell death. *J Physiol* **516** (Pt 1), 1–17.
- Fawcett DW & McNutt NS (1969). The ultrastructure of the cat myocardium. i. ventricular papillary muscle. *J Cell Biol* **42**, 1–45.
- Forbes MS & Sperilakis N (1984). Ultrastructure of mammalian cardiac muscle. In Sperilakis N, ed., *Physiology and pathophysiology of the heart*, pp. 3–42. Martinus Nijhoff Publishing, Boston.
- Kaasik A, Veksler V, Boehm E, Novotova M, Minajeva A & Ventura-Clapier R (2001). Energetic crosstalk between organelles: architectural integration of energy production and utilization. *Circ Res* **89**, 153–159.
- Kay L, Li Z, Mericskay M, Olivares J, Tranqui L, Fontaine E, Tiivel T, Sikk P, Kaambre T, Samuel JL, Rappaport L, Usson Y, Leverve X, Paulin D & Saks VA (1997a). Study of regulation of mitochondrial respiration in vivo. an analysis of influence of adp diffusion and possible role of cytoskeleton. *Biochim Biophys Acta* **1322**, 41–59.

- Kay L, Saks VA & Rossi A (1997b). Early alteration of the control of mitochondrial function in myocardial ischemia. *J Mol Cell Cardiol* **29**, 3399–3411.
- Kuznetsov AV, Tiivel T, Sikk P, Kaambre T, Kay L, Daneshrad Z, Rossi A, Kadaja L, Peet N, Seppet E & Saks VA (1996). Striking differences between the kinetics of regulation of respiration by adp in slow-twitch and fast-twitch muscles in vivo. *Eur J Biochem* **241**, 909–915.
- McCallister LP & Page E (1973). Effects of thyroxin on ultrastructure of rat myocardial cells: a stereological study. *J Ultrastruct Res* **42**, 136–155.
- Muir AR (1967). The effects of divalent cations on the ultrastructure of the perfused rat heart. *J Anat* **101**, 239–261.
- Nozaki T, Kagaya Y, Ishide N, Kitada S, Miura M, Nawata J, Ohno I, Watanabe J & Shirato K (2001). Interaction between sarcomere and mitochondrial length in normoxic and hypoxic rat ventricular papillary muscles. *Cardiovasc Pathol* **10**, 125–132.
- Ogata T & Yamasaki Y (1985). Scanning electron-microscopic studies on the three-dimensional structure of mitochondria in the mammalian red, white and intermediate muscle fibers. *Cell Tissue Res* **241**, 251–256.
- Ogata T & Yamasaki Y (1997). Ultra-high-resolution scanning electron microscopy of mitochondria and sarcoplasmic reticulum arrangement in human red, white, and intermediate muscle fibers. *Anat Rec* **248**, 214–223.
- Rassier DE, MacIntosh BR & Herzog W (1999). Length dependence of active force production in skeletal muscle. *J Appl Physiol* **86**, 1445–1457.
- Romashko DN, Marban E & O'Rourke B (1998). Subcellular metabolic transients and mitochondrial redox waves in heart cells. *Proc Natl Acad Sci U S A* **95**, 1618–1623.
- Roy RR, Pierotti DJ & Edgerton VR (1996). Skeletal muscle fiber cross-sectional area: effects of freezing procedures. *Acta Anat (Basel)* **155**, 131–135.
- Rube DA & van der Blik AM (2004). Mitochondrial morphology is dynamic and varied. *Mol Cell Biochem* **256-257**, 331–339.
- Saks V, Kuznetsov A, Andrienko T, Usson Y, Appaix F, Guerrero K, Kaambre T, Sikk P, Lemba M & Vendelin M (2003). Heterogeneity of ADP diffusion and regulation of respiration in cardiac cells. *Biophys J* **84**, 3436–3456.
- Saks V, Santos PD, Gellerich FN & Diolet P (1998). Quantitative studies of enzyme-substrate compartmentation, functional coupling and metabolic channelling in muscle cells. *Mol Cell Biochem* **184**, 291–307.
- Saks VA, Kaambre T, Sikk P, Eimre M, Orlova E, Paju K, Piirsoo A, Appaix F, Kay L, Regitz-Zagrosek V, Fleck E & Seppet E (2001). Intracellular energetic units in red muscle cells. *Biochem J* **356**, 643–657.

- Saks VA, Kuznetsov AV, Vendelin M, Guerrero K, Kay L & Seppet EK (2004). Functional coupling as a basic mechanism of feedback regulation of cardiac energy metabolism. *Mol Cell Biochem* **256/257**, 185–199.
- Schaper J, Meiser E & Stammler G (1985). Ultrastructural morphometric analysis of myocardium from dogs, rats, hamsters, mice, and from human hearts. *Circ Res* **56**, 377–391.
- Segretain D, Rambourg A & Clermont Y (1981). Three dimensional arrangement of mitochondria and endoplasmic reticulum in the heart muscle fiber of the rat. *Anat Rec* **200**, 139–151.
- Seppet EK, Kaambre T, Sikk P, Tiivel T, Vija H, Tonkonogi M, Sahlin K, Kay L, Appaix F, Braun U, Eimre M & Saks VA (2001). Functional complexes of mitochondria with Ca,MgATPases of myofibrils and sarcoplasmic reticulum in muscle cells. *Biochim Biophys Acta* **1504**, 379–395.
- Shimada T, Horita K, Murakami M & Ogura R (1984). Morphological studies of different mitochondrial populations in monkey myocardial cells. *Cell Tissue Res* **238**, 577–582.
- Sommer JR & Jennings RB (1986). Ultrastructure of cardiac muscle. In Fozzard HA, Haber E, Jennings RB, Katz AM & Morgan HE, eds., *The heart and cardiovascular system*, pp. 61–100. Raven Press, New York.
- Sun CN, Dhalla NS & Olson RE (1969). Formation of gigantic mitochondria in hypoxic isolated perfused rat hearts. *Experientia* **25**, 763–764.
- Veksler VI, Kuznetsov AV, Anflous K, Mateo P, van Deursen J, Wieringa B & Ventura-Clapier R (1995). Muscle creatine kinase-deficient mice. ii. cardiac and skeletal muscles exhibit tissue-specific adaptation of the mitochondrial function. *J Biol Chem* **270**, 19921–19929.
- Vendelin M, Eimre M, Seppet E, Peet N, Andrienko T, Lemba M, Engelbrecht J, Seppet EK & Saks VA (2004). Intracellular diffusion of adenosine phosphates is locally restricted in cardiac muscle. *Mol Cell Biochem* **256/257**, 229–241.
- Vendelin M, Kongas O & Saks V (2000). Regulation of mitochondrial respiration in heart cells analyzed by reaction-diffusion model of energy transfer. *Am J Physiol Cell Physiol* **278**, C747–C764.

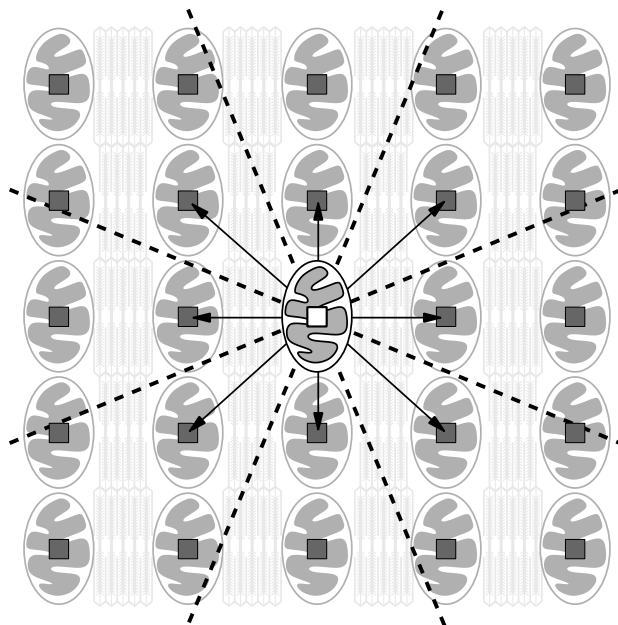


Figure 1: Schematic presentation of method of analysis of distances between mitochondrial centres. First, the centres of mitochondria are marked by small boxes. Next, the closest neighbours are found for each mitochondria, one per sector (the borders of 45° sectors are indicated by dashed lines). In the scheme, the mitochondrion, which neighbours are sought for, is highlighted. The closest neighbours for this mitochondrion are indicated by arrows. The relative coordinates of the closest neighbours, i.e. the coordinates relative to the highlighted mitochondria, are stored and analysed further.

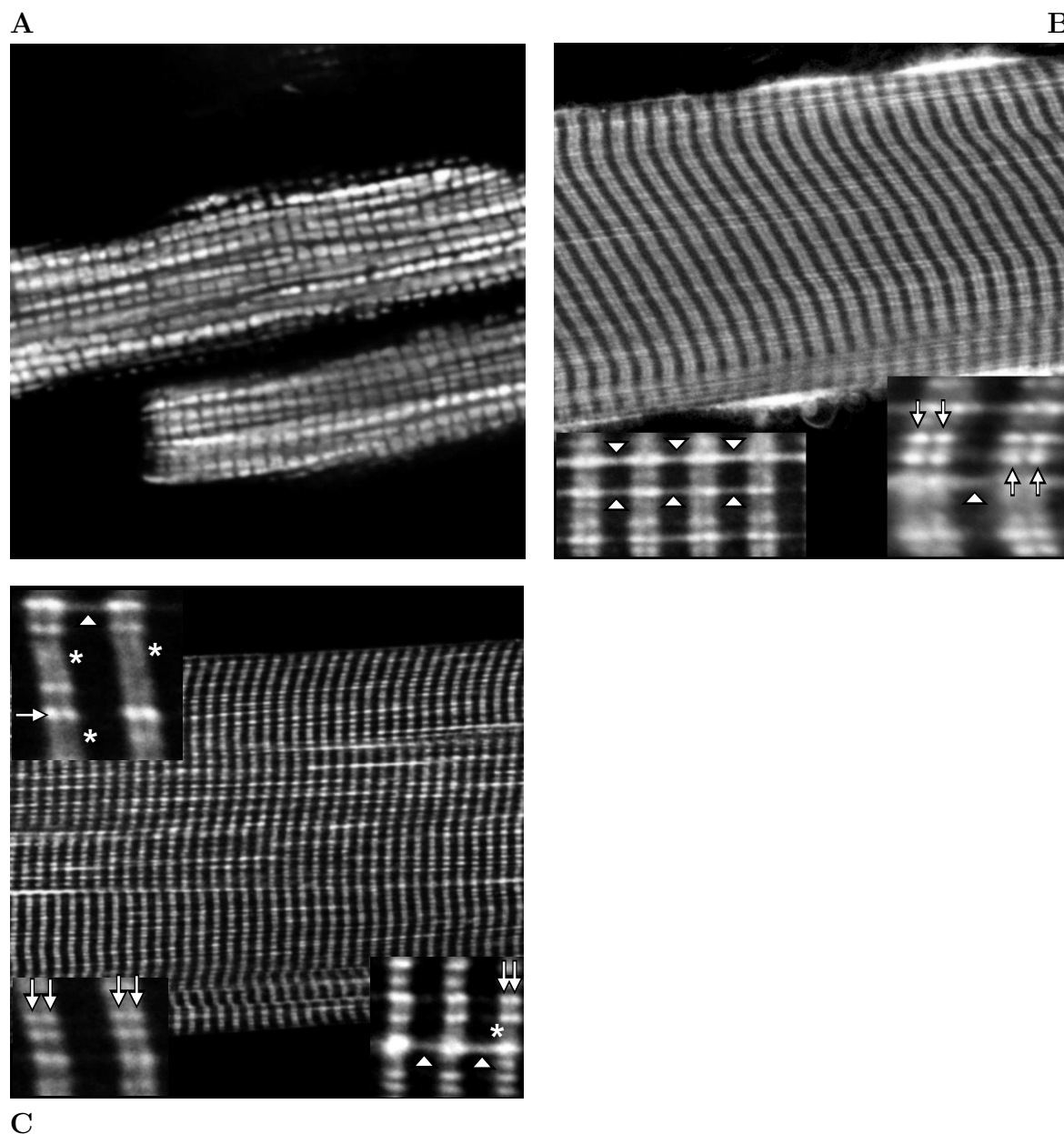


Figure 2: Representative confocal images of non-permeabilized cardiomyocytes (subplot A), soleus and white gastrocnemius fibres (subplots B and C, respectively). In these images, cardiomyocytes and the skeletal muscle fibres are oriented almost horizontally. Cardiomyocytes and soleus fibres were preloaded with MitoTracker(R) Red CMXRos; white gastrocnemius fibres were preloaded with Rhod-2. In cardiomyocytes (subplot A), mitochondria are rather regularly spaced forming a mesh covering each cardiomyocyte. In soleus and white gastrocnemius (subplots B and C, respectively), mitochondria form rows running across the fibre. These rows are formed by mitochondrial pairs, marked by arrows in the insets of the subplots B and C. On some images, “column-forming” mitochondria (Ogata & Yamasaki, 1985) can be identified (marked by arrowheads in the insets). In gastrocnemius, a long mitochondria running in pairs in transversal direction were seen occasionally (marked by “*” in the insets of subplot C). Size of the images: $59.5 \mu\text{m} \times 59.5 \mu\text{m}$ (subplot A), $94.3 \mu\text{m} \times 94.3 \mu\text{m}$ (subplot B), $14.3 \mu\text{m} \times 7.1 \mu\text{m}$ and $7.8 \mu\text{m} \times 7.8 \mu\text{m}$ (insets in the left and the right bottom corners of subplot B, respectively), $112 \mu\text{m} \times 112 \mu\text{m}$ (subplot C), $6.9 \mu\text{m} \times 6.9 \mu\text{m}$ (inset on the left top corner of subplot C), $6 \mu\text{m} \times 4.55 \mu\text{m}$ and $8.2 \mu\text{m} \times 7.6 \mu\text{m}$ (inset in the left and the right bottom corners of subplot C, respectively).

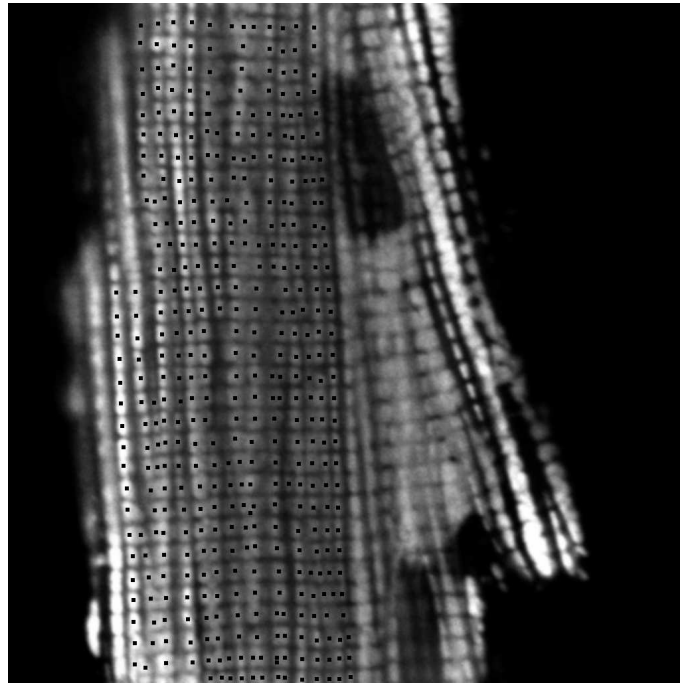


Figure 3: Representative confocal image of non-permeabilized cardiomyocyte. In this image, the cardiomyocyte is oriented vertically. The cells were preloaded with Mito-Tracker(R) Red CMXRos at 37°C. Centres of mitochondria ($n = 414$) were marked with small black boxes, as shown. Image size is $59.5 \mu\text{m} \times 59.5 \mu\text{m}$

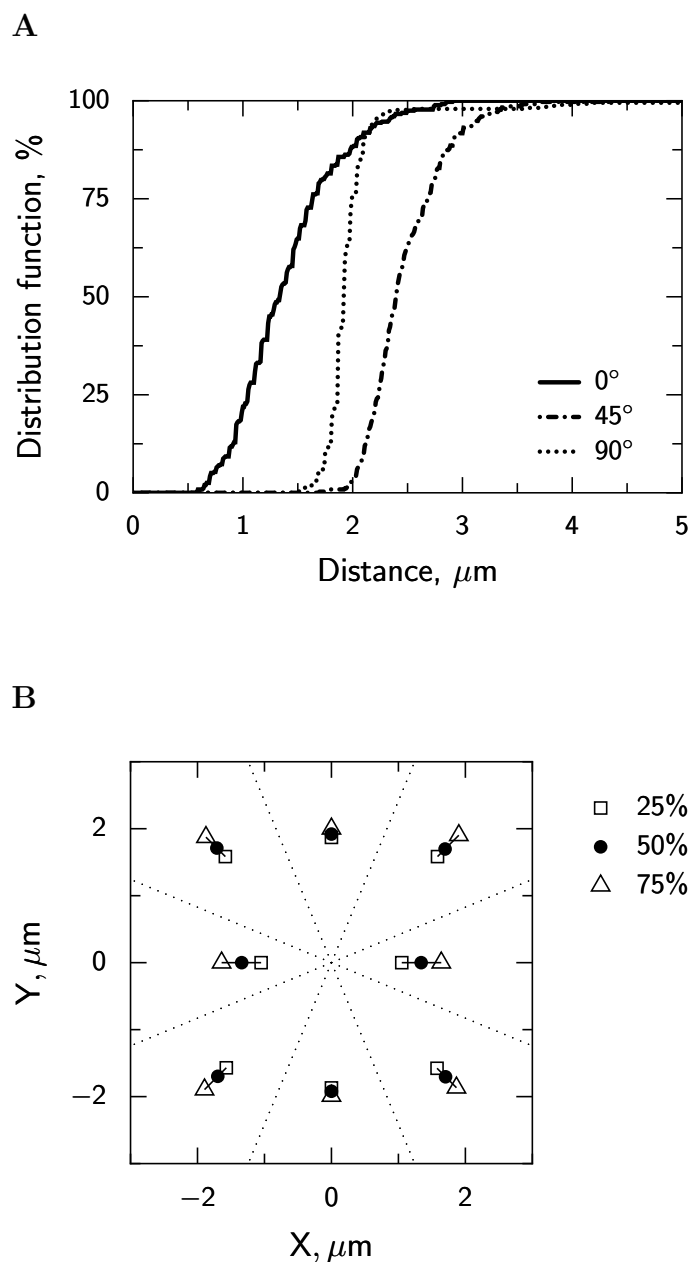


Figure 4: Distribution function (subplot A) and radial plot (subplot B) showing distribution of the distances between mitochondrial centres depending on the direction in the cardiac muscle. Here, the confocal image shown in Fig. 3 is analysed. In subplot A, the distribution functions of distance between the centres of neighbouring mitochondria along the fibre (direction 90°), in cross-fibre direction (0°), and in the diagonal direction (45°) are shown. In subplot B, the distance which enclose 25%, 50%, and 75% of neighbouring mitochondrial centres is shown in radial plot. In this plot, the distance between mitochondrial centres is given through the distance from the reference point (coordinates 0, 0) and the direction is taken equal to the middle of the corresponding sector. Sector borders are indicated by dashed lines.

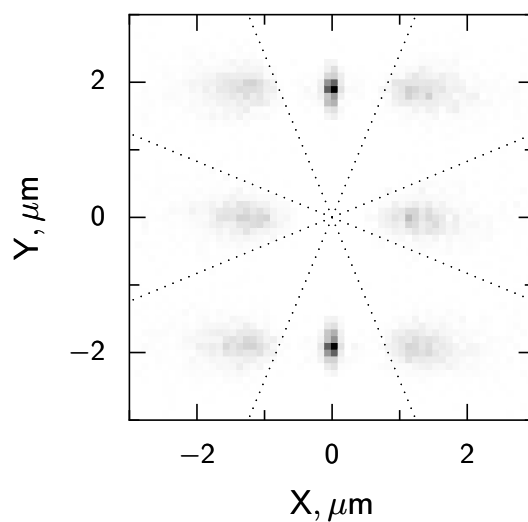


Figure 5: Distribution of centres of neighbouring mitochondria in the cardiomyocytes is analysed taking into account not only the distance but a precise direction as well. Here, $n = 10$ images are analysed with 1820 mitochondrial centres marked in the images. In the figure, probability density function is shown by colour-shades with the dark areas corresponding to large probability density values and the light areas to the small values of the density. In each sector (sector borders are indicated by dashed lines), mitochondria are not distributed evenly, but are packed in certain areas. Thus, there is a maxima of probability density surrounded by area without any significant number of mitochondrial centres.

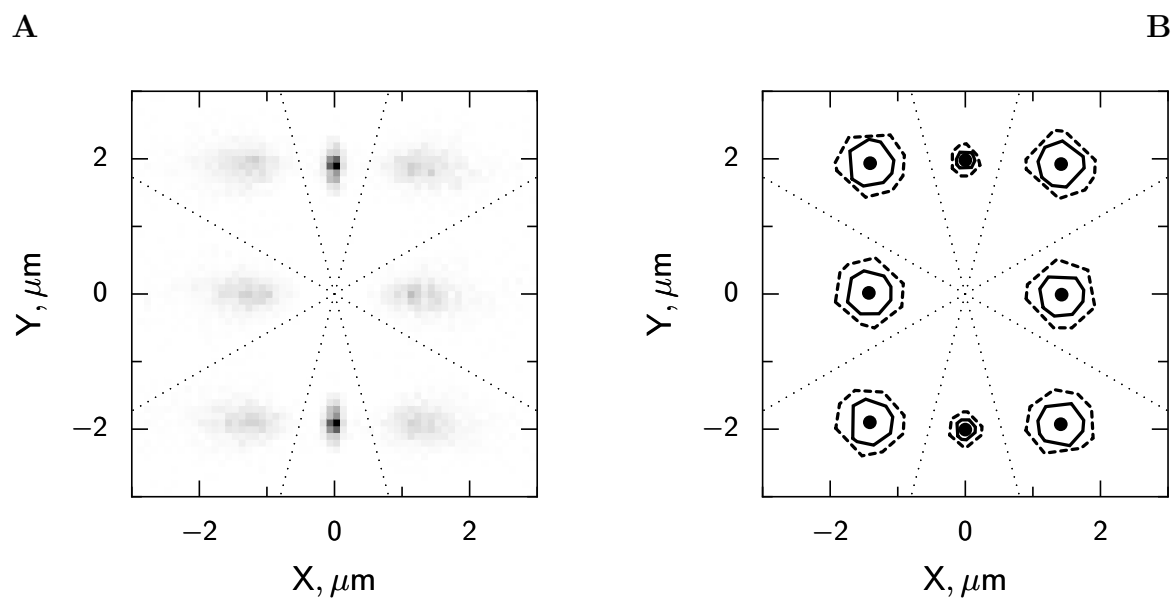


Figure 6: Distribution of centres of neighbouring mitochondria in the cardiomyocytes is analysed using the modified sectors. Here, the same images as in Fig. 5 are analysed, but with the sectors which are adjusted for analysis of cardiac muscle cell. The same notations as in Fig. 5 are used. In subplot A, probability density function is shown. Note that regions with high density of mitochondrial centres are adrift from the borders of the sectors. In subplot B, the mean position of neighbouring mitochondrial centres is shown by solid dots for each of the sectors. The area containing 50% of the centres in the sector closest to the mean position is surrounded by solid line. The similar area corresponding to 75% of the centres is enclosed by dashed line.

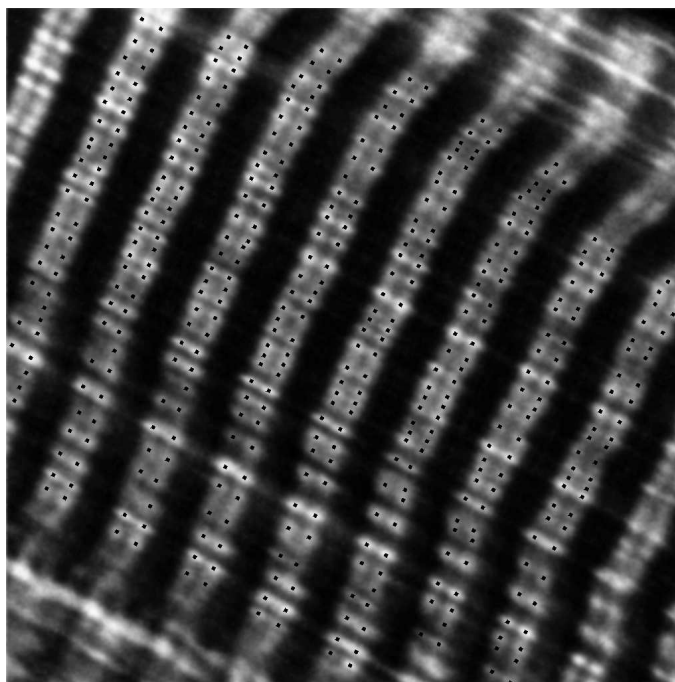


Figure 7: Representative confocal image of non-permeabilized soleus fibre. In this image, the fibre is oriented almost diagonally, with sarcomeres oriented from the top left corner to the bottom right corner of the image. The fibre was preloaded with MitoTracker(R) Red CMXRos at 4°C. Centres of mitochondria ($n = 434$) were marked with small black boxes, as shown. Image size is $29.8 \mu\text{m} \times 29.8 \mu\text{m}$.

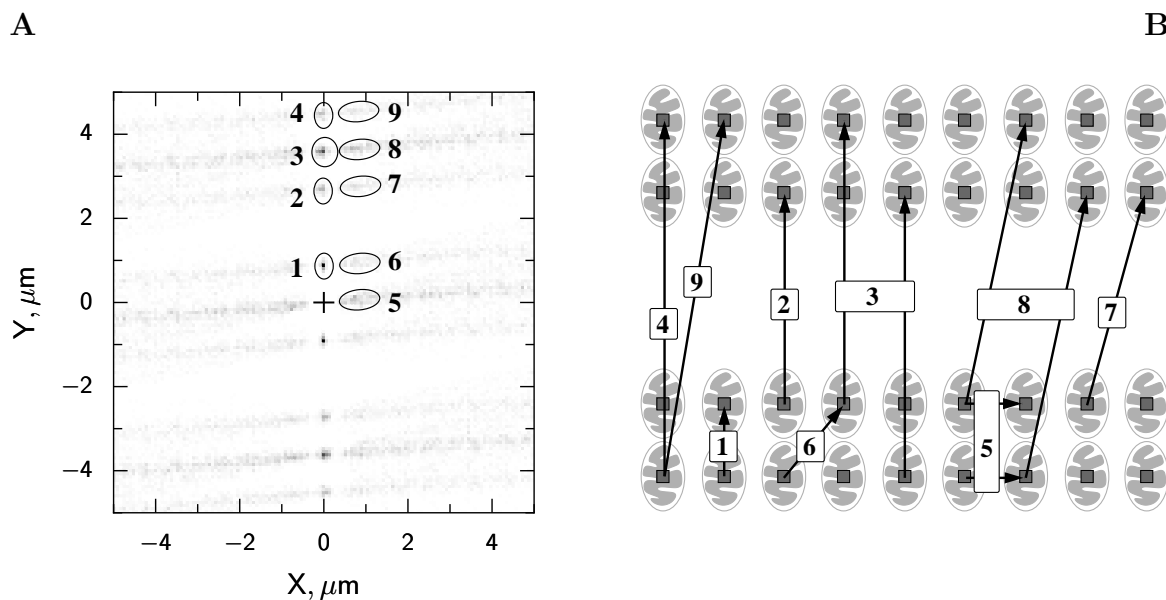


Figure 8: Probability density function describing distribution of mitochondria in soleus fibre corresponding to image shown in Fig. 7. In subplot A, the probability density function describes distribution of *all* mitochondrial centres which are within $5 \mu\text{m} \times 5 \mu\text{m}$ box from the each other. The cross in the centre of the image marks the reference point (coordinates 0, 0). Note that there are several maxima of the probability density function. The origin of the maxima marked by circles on the probability density map is explained on subplot B. In subplot B, the distances corresponding to the marked maxima are shown by arrows with the index corresponding to the maxima.

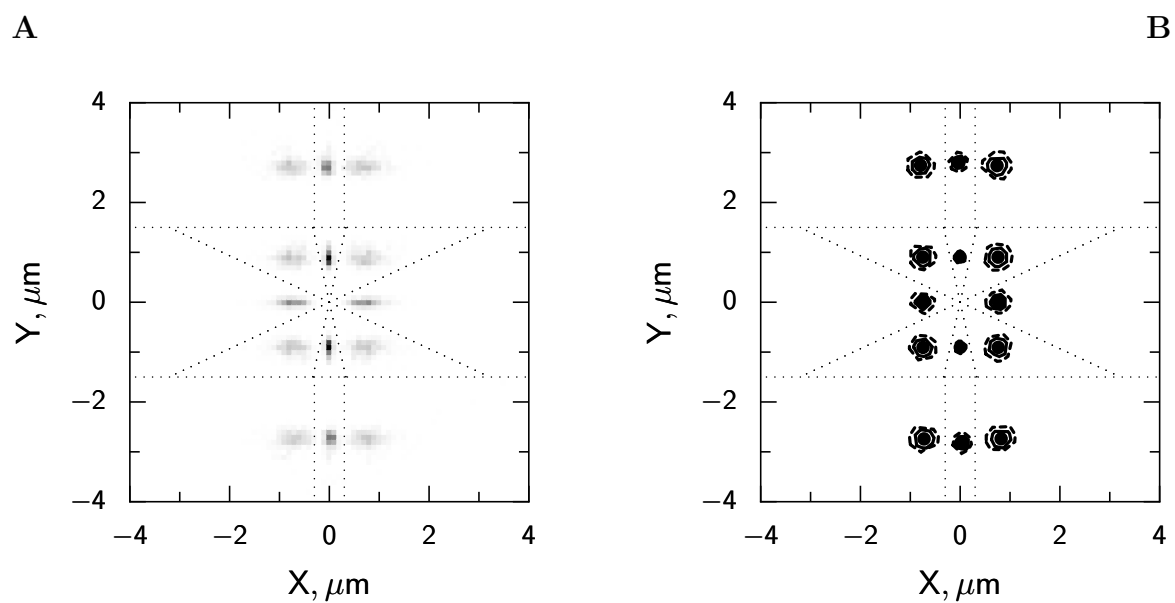


Figure 9: Distribution of mitochondria in soleus fibre. Here, $n = 10$ images are analysed with total 1659 mitochondria marked. In subplot A, probability density function is shown. In subplot B, the mean position of neighbouring mitochondrial centres is shown by solid dots for each of the sectors. The area containing 50% of the centres in the sector closest to the mean position is surrounded by solid line. The similar area corresponding to 75% of the centres is enclosed by dashed line.

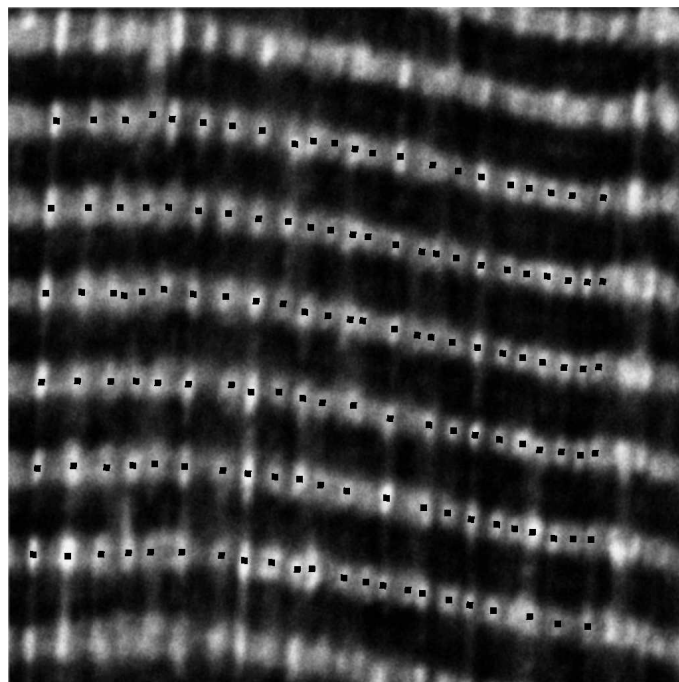


Figure 10: Representative confocal image of non-permeabilized white gastrocnemius fibre. In this image, the fibre is oriented vertically. The fibre was preloaded with Rhod-2 at 4°C. Since the distances between mitochondria within each of the pairs is considerably smaller than in soleus (see Results), we were not able to distinguish the mitochondria within the pairs in most of our images. Centres of *mitochondrial pairs* ($n = 137$) were marked with small black boxes, as shown. Image size is $25.4 \mu\text{m} \times 25.4 \mu\text{m}$.

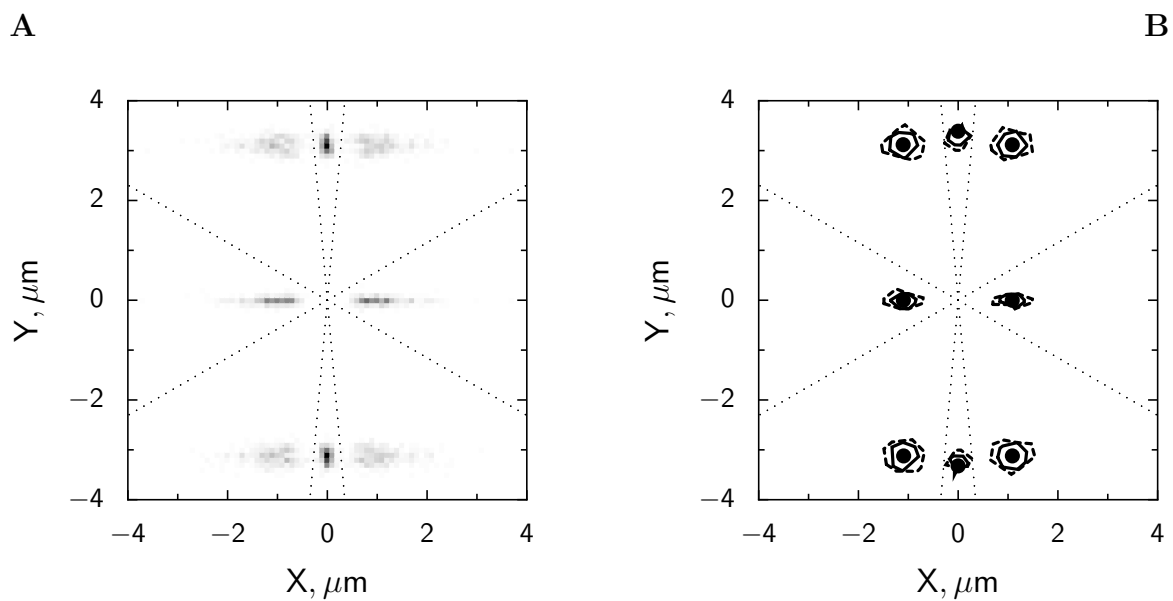


Figure 11: Distribution of *mitochondrial pairs* in white gastrocnemius fibre. Here, $n = 8$ images are analysed with total 621 mitochondrial pairs marked. In subplot A, probability density function is shown. In subplot B, the mean position of neighbouring pairs is shown by solid dots for each of the sectors. The area containing 50% of the centres in the sector closest to the mean position is surrounded by solid line. The similar area corresponding to 75% of the centres is enclosed by dashed line.